Advanced Review

# The activation strain model and molecular orbital theory

Lando P. Wolters[1,2]* and F. Matthias Bickelhaupt[1,3]*

The activation strain model is a powerful tool for understanding reactivity, or inertness, of molecular species. This is done by relating the relative energy of a molecular complex along the reaction energy profile to the structural rigidity of the reactants and the strength of their mutual interactions: $\Delta E(\zeta) = \Delta E_{\text{strain}}(\zeta) + \Delta E_{\text{int}}(\zeta)$. We provide a detailed discussion of the model, and elaborate on its strong connection with molecular orbital theory. Using these approaches, a causal relationship is revealed between the properties of the reactants and their reactivity, e.g., reaction barriers and plausible reaction mechanisms. This methodology may reveal intriguing parallels between completely different types of chemical transformations. Thus, the activation strain model constitutes a unifying framework that furthers the development of cross-disciplinary concepts throughout various fields of chemistry. We illustrate the activation strain model in action with selected examples from literature. These examples demonstrate how the methodology is applied to different research questions, how results are interpreted, and how insights into one chemical phenomenon can lead to an improved understanding of another, seemingly completely different chemical process. 

**How to cite this article:**
*WIREs Comput Mol Sci* 2015, 5:324–343. doi: 10.1002/wcms.1221

## INTRODUCTION

Chemistry is, roughly speaking, the branch of the natural sciences investigating the properties, composition, and transformation of matter. Within theoretical chemistry, this is done not by observation, but by a mathematical description of the physical system of interest. The constant improvement in the quality of mathematical descriptions, combined with the enormous advancement of computer technology in the past decades, has allowed the field of theoretical chemistry to advance as well. Nowadays, it is feasible to computationally study a large variety of molecular systems and chemical processes with, for many purposes, sufficient accuracy. Although some of the romance of doing practical experiments is lost, theoretical chemistry opens up a whole new world of research by eliminating many practical limitations. Theoreticians can, for example, study a synthetically useful and thus desired type of reaction which, however, does not proceed. Such a reaction can not be studied experimentally because it does not occur. Theory, on the other hand, can examine this process *in silico* and therefore reveal the reasons *why* it is not viable and what can be done to change this situation for the better.

In the following, we focus on understanding chemical reactivity, i.e., the reaction energy profile that accompanies the transformation of molecular species into new species. We will assume that the energy

*Correspondence to: F.M.Bickelhaupt@vu.nl, L.P.Wolters@vu.nl

[1]Department of Theoretical Chemistry and Amsterdam Center for Multiscale Modeling (ACMM), VU University Amsterdam, Amsterdam, The Netherlands

[2]Dipartimento di Scienze Chimiche, Università degli Studi di Padova, Padova, Italy

[3]Institute of Molecules and Materials (IMM), Radboud University Nijmegen, Nijmegen, The Netherlands

Conflict of interest: The authors have declared no conflicts of interest for this article.

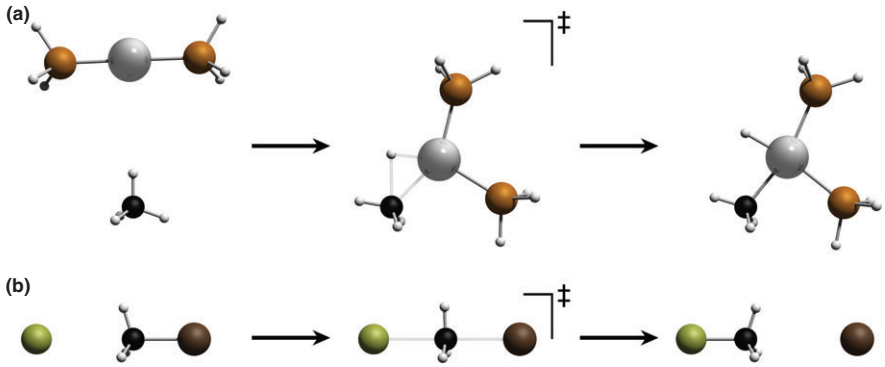


**FIGURE 1** | Schematic representation of (a) oxidative addition and (b) $S_N2$ reaction mechanisms.

profile of a chemical reaction has been obtained to sufficient accuracy, and will discuss the application of the activation strain model of chemical reactivity,[1–5] which has been developed to obtain more insight into the qualitative and quantitative features of the energy profile. This is done by splitting the relative energy of a molecular complex along the reaction coordinate into two separate terms, originating from the deformation of the reacting species and the interaction between them. Similar approaches have been explored before,[6–8] but have not evolved into the generally applicable model that the activation strain model, as it is known in short, has become. Note also, that more recently the group of Houk has adopted the same approach, the distortion/interaction model, differing only in terminology.[9]

Conveniently, there is no special computer code required to perform activation strain analyses: all necessary quantities can be computed using any of the regular quantum-chemical software packages available. As a result, the activation strain model has been applied by various research groups, on a range of chemical processes, such as nucleophilic substitution,[1,10–19] cycloaddition,[20–33] oxidative addition,[34–49] isomerization,[50–55] and many other processes from organic[56–69] and organometallic[70–91] chemistry.

The activation strain model has been around for a number of years and has been reviewed before.[3,5] In this advanced review, we will therefore place extra emphasis on how this model connects to the well-known, and even more mature, framework of quantitative (frontier) molecular orbital (MO) theory.[92–97] We limit our discussion primarily to $S_N2$ and oxidative addition reactions (Figure 1(a) and (b), respectively), but discuss related chemical processes when relevant. Also, we limit ourselves to analyses of gas-phase results, to avoid complications introduced by solvation effects. These complications arise from the fact that one has to take into account the partial desolvation that occurs at the interacting sites of approaching reactants. It should be noted that this is inherent to any fragment-based description, and that solutions have been proposed.[41,98]

## THE ACTIVATION STRAIN MODEL

The activation strain model[1–3,5] is a fragment-based approach, and the first necessary step is therefore to choose suitable reference fragments. There is freedom of choice, but for the bimolecular processes that we will be dealing with in the following sections, the obvious and straightforward choice is to use the initial reactants as reference fragments. For bimolecular reactions via a transition state (TS), the activation strain model can be used to obtain insight into, for example, the height of a reaction barrier. This is done by splitting its energy at this point, $\Delta E^{\ddagger}$, into the strain energy term $\Delta E^{\ddagger}_{\text{strain}}$, and the interaction energy term $\Delta E^{\ddagger}_{\text{int}}$:

$$\Delta E^{\ddagger} = \Delta E^{\ddagger}_{\text{strain}} + \Delta E^{\ddagger}_{\text{int}}. \quad (1)$$

The strain energy $\Delta E^{\ddagger}_{\text{strain}}$ is the energy required for the geometrical deformations of the fragments from a reference geometry (often, but again not necessarily, their equilibrium geometry) to the geometry they acquire at the transition state. It is therefore strongly related to the structural rigidity of the fragments. As the reference geometries are usually not distorted, this term is typically destabilizing. In principle, the strain term can also incorporate excitations to electronic configurations that are better suited or required for the interaction studied, but most often the reference fragments are chosen as already having the correct valence configuration. The strain term can readily be split further into separate contributions from each reactant.

The interaction energy $\Delta E^{\ddagger}_{\text{int}}$ accounts for all chemical interactions as they arise when the structurally deformed reactants are brought from infinity

  

to their positions in the transition state geometry and allowed to interact. It comprises all the energetic effects that result from combining and mixing the charge distributions of the fragments. Often, this term is further dissected using an energy decomposition scheme, of which many are available. We will elaborate on this term in the next section.

The activation strain model can be generalized to any point along an energy profile. The relative energy $\Delta E$, as well as its components, then becomes functions of the reaction coordinate $\zeta$ and Eq. (1) generalizes to

$$\Delta E(\zeta) = \Delta E_{\text{strain}}(\zeta) + \Delta E_{\text{int}}(\zeta). \qquad (2)$$

When applied to an energy profile of a chemical reaction with a central reaction barrier, all terms start at a value close to zero, but not necessarily at zero. This is because a reaction (in the gas-phase) typically starts from a precursor complex, in which the fragments are slightly distorted (small $\Delta E_{\text{strain}}$) and interact only weakly (small $\Delta E_{\text{int}}$). From there on, the reactants become increasingly deformed along the reaction coordinate, leading to a continuously increasing strain energy $\Delta E_{\text{strain}}$. Concomitantly, the interaction between the fragments usually strengthens, which leads to the interaction energy $\Delta E_{\text{int}}$ becoming more stabilizing along the reaction profile. At the point where the destabilization from the strain term increases at the same rate as the stabilization from the interaction energy term strengthens, that is, $dE_{\text{strain}}(\zeta)/d\zeta = -dE_{\text{int}}/d\zeta$, the derivative of the total energy profile with respect to the reaction coordinate is zero ($dE/d\zeta = 0$). At this point, the energy profile achieves either a maximum (the reaction barrier), where the transition state occurs, or a minimum.

It follows that, to elucidate heights of reaction barriers or stability of stationary points, one should not only consider the rigidity of the fragments and the strength of their mutual interaction, but also their position along the reaction coordinate, and therefore the slopes of the strain and interaction terms.[2] Depicted in Figure 2 is a comparison of the activation strain analyses of two generic chemical reactions to exemplify this. In this comparison, the strain curves $\Delta E_{\text{strain}}(\zeta)$ resulting from both reactions are chosen to be equal, while the interaction curves $\Delta E_{\text{int}}(\zeta)$ are different. From Figure 2, it is easily concluded that, upon going from the first reaction (black lines) to the second reaction (red lines), the energy profile $\Delta E(\zeta)$ is shifted up in energy, due to a weaker interaction between the fragments. The result is a higher reaction barrier, which is shifted to the product side because the interaction energy curve is descending less steeply. This is in agreement with the Hammond postulate,[99] which

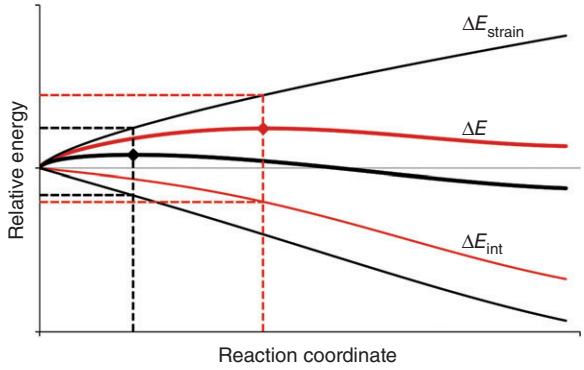


**FIGURE 2 |** Comparison of generic activation strain analyses of two different reactions. The dashed lines indicate the results from a single-point analysis at the transition state geometry.

indeed follows naturally from the activation strain model. Note, however, that an analysis at the transition state geometries only, as indicated by the dashed lines, can be misleading, as in this case one would conclude that the reaction barrier becomes higher due to a significant increase in strain energy, and even despite (!) a slightly more stabilizing interaction between the fragments.

Although analyses along full reaction paths (or critical sections thereof) are more insightful than single-point analyses at the transition state only, there are still a number of important factors to take into account in order to avoid misleading results. First, analyses of two similar reactions are more readily compared when the energy profiles are projected onto a critical geometrical parameter. Again, one can choose freely, but to arrive at insightful results, the parameter should be well-defined along the reaction profile and be sufficiently descriptive for the overall reaction process, as well as undergo considerable changes in the transition state region.[100] Second, the total energy profile is the sum of two contributions that are not orthogonal and thus influence each other. The strain term, for example, is almost always positive as a consequence of its very definition. Eliminating the strain term by freezing the geometries of the fragments and pushing them toward each other, however, would not lead to a lower total energy profile. Instead, the interaction term would weaken and, as it includes a repulsive component as well, eventually become repulsive, likely raising the relative energy profile to higher values than the initial energy profile that was obtained with relaxed geometries. Thus, a significant part of the interaction energy that is built up during the reaction, requires a certain amount of geometrical deformation, and thereby strain energy. This balance between mutually dependent terms in itself is not problematic, but should be kept in mind when applying any model that

  

contains interacting and opposing components. To get insight into the importance of this interplay, it can be useful to use additional analyses where (part of) the geometries are fixed.[10,11,44,87,101–104] This prevents any perturbation stemming from geometry changes of the fragments that could easily hide a more clear picture of the electronic interactions.

In this review, we will focus exclusively on bimolecular processes, but it is worth mentioning that the activation strain model can also be used to study unimolecular processes.[51,67,86,101] When chemically meaningful fragments can be discerned, the relative energy $\Delta E$ of the molecular structure is given by the sum of the change, during the process, in strain energy within the fragments and the change in interaction between these two fragments: $\Delta E(\zeta) = \Delta\Delta E_{\text{strain}}(\zeta) + \Delta\Delta E_{\text{int}}(\zeta)$.

Furthermore, it should be noted that an understanding of the energy profile of a certain process does not necessarily lead to a complete picture of the chemical phenomenon being investigated. Obviously, the activation strain model does not aim to explore, let alone explain, dynamic effects on the reactivity. Nor does it render unnecessary the search for alternative reaction pathways, or competitive reactions.

## MOLECULAR ORBITAL THEORY AND INTERACTION ENERGY DECOMPOSITION

The activation strain model provides great insight into relative energies of transition states and even entire reaction energy profiles, as it enables us to ask the very relevant question why a certain geometrical deformation leads to an energetic destabilization, or why molecular fragments can build up a particular mutual interaction. Thus, to achieve a genuine explanation of the phenomena of interest, the reasons behind these changes in strain and interaction energy can be subjected to further investigation using quantitative (Kohn–Sham) MO theory.[94–97,107,108]

As discussed in the previous section, the strain energy of a fragment is the energy needed for the geometric deformations of the fragments, relative to a reference geometry. As this reference geometry is typically the equilibrium geometry of the fragment, the amount of strain energy is often directly related to the amount of geometrical distortion, and can be readily linked to the extent to which, for example, bonds are stretched or angles have changed. Further explanation is therefore not always needed. However, when required, MO theory can help to understand why a certain geometric deformation leads to a less stable molecular species. This is because changes in the total energy of the molecular fragment tend to parallel the changes in the sum of its orbital energies, and the orbital energies are again altered by changes in the molecular geometry. Thus, by investigating the dependence of the orbital energies on a geometrical parameter of interest, as is done in Walsh diagrams, one can explain why a certain molecular deformation leads to a destabilization of the molecular fragment. In a subsequent step, one can of course divide the fragment itself into smaller fragments, and provide an explanation for, for example, a rise in the orbital energy in terms of a decreased in-phase or increased out-of-phase overlap of the orbitals of the smaller fragments. This process can be repeated until the explanation is provided in terms of atomic orbitals, which no longer have any geometry dependence. Luckily, a satisfactory level of understanding is usually achieved at an earlier stage, based on the transferability of properties of common functional groups.

To obtain insight into the interaction energy $\Delta E_{\text{int}}$, it is usually split into separate terms arising from different types of interactions, in order to get a quantitative idea of their contributions to the total interaction energy. Such an interaction energy decomposition scheme is a useful tool to get insight into the relative importance of the different types of contributing interactions, and many different varieties have been developed.[109–114] Any decomposition of the interaction energy into separate terms is artificial, so in principle one cannot go wrong when choosing one (Box 1). Some schemes, however, may be more suitable than others for certain applications. In the following, we will discuss the energy decomposition analysis (commonly abbreviated EDA) as implemented in the Amsterdam Density Functional (ADF) software package.[107,115,116] We choose this scheme for its transparent, easy-to-understand nature, as it dissects the interaction energy into terms that directly correspond with a causal bonding mechanism in MO theory. This last step is of crucial importance, because interaction energy decomposition schemes are just quantitative tools, and numerical data provided by such schemes should not be interpreted as the final answer to a question, nor be presented as such.

The EDA approach is based on that of Morokuma[117,118] and the extended transition state (ETS) method developed by Ziegler and Rauk.[119–121] Within this scheme, the interaction energy $\Delta E_{\text{int}}$ is decomposed into three terms, that can be interpreted physically meaningfully and quantitatively accurately in the framework of the MOs arising from Kohn–Sham density functional theory:

$$\Delta E_{\text{int}} = \Delta V_{\text{elstat}} + \Delta E_{\text{Pauli}} + \Delta E_{\text{oi}}. \quad (3)$$

  

## BOX 1

### THEORIES, MODELS, AND THE SCIENTIFIC METHOD. A SEMANTIC INTERMEZZO

Here we shortly discuss the meaning of the terms 'theory' and 'model', which feature prominently in the title of this review, and appear regularly throughout its contents. The following is a word of caution to keep in the back of one's mind, and certainly not an attempt to provide a definitive view on theories and models and their application within the scientific method.

Colloquially, the word 'theory' often refers to a hypothesis, or just a speculative idea.[105] But in science, a 'theory' is more aptly described as 'a well-substantiated explanation of some aspect of the natural world, based on a body of facts that have been repeatedly confirmed through observation and experiment'.[106] Clearly, the term gets an entirely different meaning when changing context! This is why it is nonsensical to state that, for example, 'the theory of evolution is just a theory', as it fallaciously equivocates on the two different meanings. But how does this relate to the field of 'theoretical' chemistry, or density functional 'theory', or molecular orbital 'theory'? Here, we encounter a third meaning of the term, where it refers to a mathematical framework, derived from a set of postulates, which is intended to make predictions of physical results.

The data obtained using, for example, density functional theory, can be interpreted using models. A model, within scientific context, can be described as an 'idealized description of a particular system, situation, or process, often in mathematical terms, that is put forward as a basis for theoretical or empirical understanding'.[105] Within the field of theoretical chemistry, there are many discussions centered around the use of models. Given that a model is an idealized, often simplified, description, and therefore inherently 'false', it should be judged on the basis of its usefulness: the quality of its predictions, general applicability, ease of understanding, and revelation of causal relationships, etc. Unfortunately, however, many of the discussions focus on particular individual components of a model. The main cause of the debates is therefore often not the model itself, but rather the overinterpretation of its results.

Similar to the generalization of the $\Delta E_{\text{int}}$ term to any point along an energy profile (as discussed in the previous section, see Eqs (1) and (2)) also this equation can be generalized to the entire reaction profile, again making each term a function of the reaction coordinate $\zeta$.

For the discussion of the individual terms contributing to the interaction energy $\Delta E_{\text{int}}$, the formation of AB is considered from two fragments, A and B, which, as discussed in the previous section, already have the geometry and electronic configuration corresponding to the combined complex AB. These fragments have electronic densities $\rho^{\text{A}}$ and $\rho^{\text{B}}$, with corresponding wavefunctions $\Psi^{\text{A}}$ and $\Psi^{\text{B}}$ and energies $E^{\text{A}}$ and $E^{\text{B}}$. The first term, $\Delta V_{\text{elstat}}$, is the classical electrostatic interaction between the fragments as they are brought from infinity to their positions in the complex AB, giving rise to the sum density $\rho^{\text{A+B}} = \rho^{\text{A}} + \rho^{\text{B}}$, and corresponding Hartree product wavefunction $\Psi^{\text{A}}\Psi^{\text{B}}$. It consists of the Coulombic repulsion between the nuclei $\alpha$ and $\beta$ (at positions R, with charge Z) of the fragments A and B, respectively, as well as the repulsion between their unperturbed electron densities $\rho^{\text{A}}$ and $\rho^{\text{B}}$, and the attractive interactions between the nuclei of one fragment with the electron density of the other fragment:

$$\begin{aligned}\Delta V_{\text{elstat}} = &\sum_{\alpha\in A}\sum_{\beta\in B}\frac{Z_\alpha Z_\beta}{R_{\alpha\beta}} \\ &- \int \sum_{\alpha\in A}\frac{Z_\alpha\,\rho^{B}(r)}{|R_\alpha - r|}\mathrm{d}r - \int \sum_{\beta\in B}\frac{Z_\beta\,\rho^{A}(r)}{|R_\beta - r|}\mathrm{d}r \\ &+ \int\int \frac{\rho^{A}(r_1)\,\rho^{B}(r_2)}{r_{12}}\,\mathrm{d}r_1\mathrm{d}r_2\,. \end{aligned} \tag{4}$$

It is known from elementary electrostatics that two interpenetrating charge clouds have a repulsion that is smaller than the one between point charges at their centers, from which follows that fragments consisting of electronic densities around positive nuclei will typically experience a net attraction. Thus, $\Delta V_{\text{elstat}}$ is usually attractive for molecular fragments at chemically relevant distances. It is important to remember that this term is computed from frozen electron densities $\rho^{\text{A}}$ and $\rho^{\text{B}}$, obtained by optimizations in absence of the other fragment.

The Pauli repulsion, $\Delta E_{\text{Pauli}}$, is the energy change that occurs upon going from the product wavefunction $\Psi^{\text{A}}\Psi^{\text{B}}$ to an intermediate wavefunction $\Psi^0$, that, after antisymmetrization by an operator $\hat{\text{A}}$ and renormalization by a constant $N$, properly obeys the Pauli principle: $\Psi^0 = N\hat{\text{A}}\,\{\Psi^{\text{A}}\Psi^{\text{B}}\}$. This intermediate state, with density $\rho^0$, has energy $E^0$, such that $\Delta E^0 = E^0 - E^{\text{A}} - E^{\text{B}} = \Delta V_{\text{elstat}} + \Delta E_{\text{Pauli}}$ and $\Delta E_{\text{Pauli}} = \Delta E^0 - \Delta V_{\text{elstat}}$. The Pauli repulsion comprises the repulsive interaction between electrons

  

having the same spin. It is responsible, for example, for the four-electron destabilizing interactions between doubly occupied orbitals from the different fragments. This is the origin of steric repulsion: when two occupied valence orbitals from different fragments overlap, antisymmetrization results in a nodal plane. The large gradients in this region significantly increase the kinetic component of the orbital energies. In the past, the Pauli repulsion term has been criticized for being based on an 'arbitrarily chosen, nonphysical reference state', and resulting from 'first violating the Pauli principle and then imposing it'.[122,123] Such statements may, at times, be relevant reminders for the overenthusiastic user of the decomposition scheme, but serve no further purpose as they themselves are examples of overinterpretation: all terms are defined as they are, and produce the numbers that follow from these clear and transparent definitions (Box 1).

In the final step of the bond formation between fragments A and B, the system is allowed to relax from $\Psi^0$, and corresponding $\rho^0$, to the final $\Psi^{AB}$ and optimized density $\rho$ of the molecular complex AB. The accompanying energy change is the orbital interaction term: $\Delta E_{oi} = E^{AB} - E^0$. This term is by definition stabilizing, because it involves an optimization. More specifically, it allows the virtual orbitals on the fragments to be mixed in, and therefore includes HOMO–LUMO (highest occupied molecular orbital and lowest unoccupied molecular orbital, respectively) interactions. As a result of this mixing, the orbital interaction component contains the stabilizing contributions from polarization of the fragments A and B, as well as charge transfer between the fragments. It is hard, if not impossible, to rigorously distinguish polarization from charge transfer. This is therefore not attempted in this interaction energy decomposition scheme (in contrast to the scheme of Morokuma[117,118]). However, when using a fragment-based approach and further orbital analyses, it is possible to get insight into the two individual contributions at least partially. Both polarization and charge transfer will show up as occupied-virtual orbital mixing, but in the case of polarization, the occupied and virtual orbitals will be localized on the same fragment, whereas charge transfer will show up as the mixing of occupied orbitals on one fragment with unoccupied orbitals on the other fragment. Besides detailed orbital analyses, additional electron density analyses (based on atomic charge analyses, the deformation density, etc.) can also contribute to distinguish between polarization and charge transfer.

Furthermore, it follows from group theory that only orbitals of the same symmetry, that is, the same character under the available symmetry operations, can interact and mix. This allows for a further decomposition of the total orbital interaction energy $\Delta E_{oi}$ into contributions from each irreducible representation $\Gamma$ of the point group to which the molecular system belongs[120]:

$$\Delta E_{oi} = \sum_{\Gamma} E_{oi}^{\Gamma}. \tag{5}$$

Finally, when the functional is augmented with an explicit correction to account for dispersion interactions, the contribution $\Delta E_{disp}$ from this correction term is simply added to Eq. (3) as an additional component of the interaction energy $\Delta E_{int}$. In Figure 3, schematic orbital interaction diagrams are shown for the different types of orbital interactions that play a main role throughout this review.

After this rigorous numerical treatment, explanations are often presented schematically, using generic hydrogen-like atomic orbitals and a few core concepts from MO theory, further aided by symmetry considerations derived from group theory. A number of elementary atomic properties, such as electronegativity and atomic radii, can easily be taken into account, using what is in essence a perturbative treatment. Thus, although the results are derived from state-of-the-art density functional theory computations and detailed analyses, the final explanation often shows the essence of the phenomenon of interest in a pictorial manner that is easy to memorize, to communicate, and to apply to new situations.

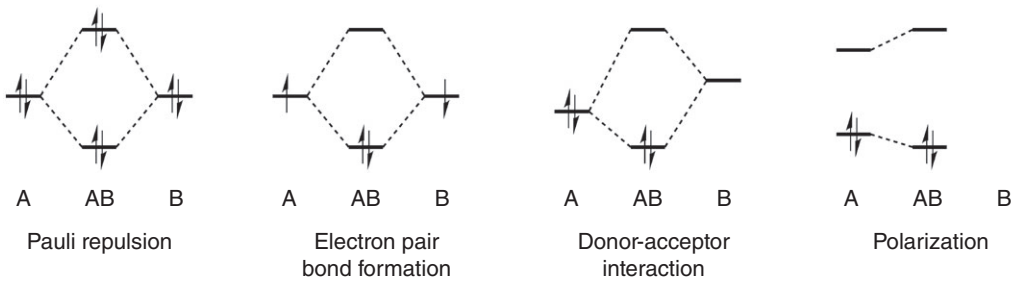


**FIGURE 3** | Orbital interaction diagrams for the most commonly appearing interactions.

  

Such representations nevertheless accurately account for the observations made, and provide important insights. In the past, this approach, and MO theory in general, has proven to be very powerful for explaining many observations made in a variety of fields in chemistry, limited not only to molecules, but also including solids.[94–97,124]

## SELECTED APPLICATIONS

In this section, we take the reader through some representative examples from the scientific literature, in which the activation strain model plays a prominent role. We will draw parallels between different chemical processes, and, when appropriate, focus on important related aspects, such as a more detailed view on the structural properties of the transition metal catalysts applied in oxidative addition.

### Palladium-Mediated C—H Activation

We start our discussion of applications with the oxidative addition of a methane C—H bond to an uncoordinated Pd metal center. This model reaction represents general Pd-catalyzed bond activation reactions that are of paramount importance in modern synthesis.[125] Palladium-catalyzed methane activation starts from a weakly bound reactant complex, and proceeds via a reaction barrier in which the C—H bond is stretched, to a product complex where the C—H bond is effectively broken, and new Pd—C and Pd—H bonds are formed[35,47,126] (see also Figure 1(a)). The energy profile is shown in Figure 4 in black lines (we return to the blue and red lines later). Here, the fragments are the reactants Pd and $CH_4$, and the stretch of the activated C—H bond is chosen as the reaction coordinate.[100]

It becomes clear from this graph that, as the reaction proceeds, the strain term $\Delta E_{strain}$ becomes monotonically and increasingly destabilizing. This is not surprising, as the reaction involves rupture of a chemical bond and the energy is projected on the amount by which this bond is stretched. The strain term in this case matches the methane C—H dissociation curve closely, because the only significant contribution to $\Delta E_{strain}$ stems from $H_3C$—H stretching, which destabilizes the bonding $\sigma_{C—H}$ orbital due to a decreased in-phase overlap of the $CH_3^\bullet$ $sp^3$ lobe (note that we use the '$sp^3$' moniker only as a general description of this orbital's shape, not its exact composition) with the $H^\bullet$ 1s orbital. The true dissociation curve is slightly lower in energy than the strain curve, because the $CH_3^\bullet$ moiety has more freedom to relax, whereas during the reaction there are additional small geometrical changes in the $CH_3^\bullet$ moiety induced by the presence of the Pd center, which occur to lower the Pauli repulsion between the fragments. The contribution to the strain term from the monatomic Pd fragment itself, however, is zero, as follows from the definition.

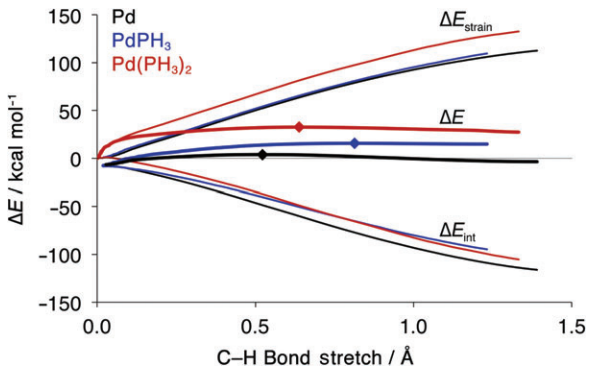


**FIGURE 4 |** Activation strain analyses for the oxidative addition of methane to Pd (black), $PdPH_3$ (blue), and $Pd(PH_3)_2$ (red). A dot designates a TS. Energies and bond stretch are relative to reactants.

The interaction energy curve starts just below zero, because the moderate Pauli repulsion is compensated for by the sum of the electrostatic attraction and the orbital interactions. At this stage of the reaction, the stabilizing orbital interaction term originates primarily from electron donation from the occupied orbitals on the methane substrate to the empty 5s acceptor orbital on Pd. As the reaction proceeds, the Pd intrudes into the space of the $CH_4$ fragment, strengthening all components of $\Delta E_{int}$. Firstly, $\Delta V_{elstat}$ becomes more strongly stabilizing simply because the electronic densities of the fragments get closer to the nuclei of the other fragment. At the same time, the overlap between the occupied orbitals on both fragments increases, leading to a stronger Pauli repulsion $\Delta E_{Pauli}$. The orbital interaction $\Delta E_{oi}$ becomes more strongly stabilizing (more negative), primarily due to a different donor–acceptor interaction that comes into play. As the C—H bond is stretched and the $\sigma^*_{C—H}$ LUMO is stabilized, the Pd fragment migrates to a position where one of its occupied 4d orbitals has favorable overlap with this $\sigma^*_{C—H}$ orbital. This provides a backbonding interaction, where charge is being donated from the metal to the substrate, in accord with the oxidative nature of this reaction. Population of the $\sigma^*_{C—H}$ orbital leads to C—H bond breaking, and the in-phase overlap of the Pd 4d orbital with this $\sigma^*_{C—H}$ orbital results in the newly formed Pd—C and Pd—H bonds.

Proceeding from this starting point, we will introduce modifications to the reaction system, and compare the results to see how these modifications influence the different energy terms, and thereby the overall energetics of the reaction. We start with a brief

  

study on ligand effects by investigating the oxidative addition of the methane C—H bond to $PdPH_3$.

## Ligand Effects on Palladium-Mediated C—H Activation

The energy profile of oxidative methane addition to monocoordinated $PdPH_3$ is shown in Figure 4. The reaction profile starts from a similar reactant complex as for the bare Pd catalyst, but becomes progressively higher in energy (compare black and blue lines).[47] Activation strain analyses reveal that this difference is caused by a weaker catalyst–substrate interaction, while the structural deformations are very similar. The latter is a straightforward result, as the substrate goes through the same geometrical transformation, and this is still the main source of strain energy $\Delta E_{strain}$. The contribution from the catalyst is close to, but no longer exactly zero, as there is a minor contribution originating primarily from a slight elongation of the Pd—$PH_3$ bond length, caused by a small donor–acceptor interaction between occupied orbitals on $CH_4$ to the LUMO of $PdPH_3$, which has antibonding character along the Pd—$PH_3$ bond.

The more important consequence of introducing the $PH_3$ ligand is the weaker $\Delta E_{int}$, which translates directly into a higher reaction barrier and less stable product complex. Note that the less steeply descending interaction energy curve translates not only in a higher reaction barrier, but also shifts the transition state to the product side. The weakening of the interaction energy is the net result of a weakening of all its components (results not shown), which can be explained by the effect of the $PH_3$ ligand on the electronic structure of the Pd center. $PH_3$ is a moderately $\pi$-accepting ligand, and as such depletes some of the electron density from the Pd center in $PdPH_3$ via $\pi$ backdonation. This not only leads to less electrostatic attraction between the $PdPH_3$ fragment and the substrate, but also decreases the overlap of occupied orbitals on both fragments, which reduces Pauli repulsion and compensates for the decreased electrostatic attraction. However, the $\pi$ backbonding from Pd to $PH_3$ also stabilizes the d orbitals on Pd, most notably the $d_{xz}$ and $d_{yz}$ (with the Pd—P bond being the z-axis). This includes the d orbital that donates into the substrate $\sigma^*_{C—H}$ orbital, which is one of the main contributing factors to the orbital interactions $\Delta E_{oi}$. Lowering the energy of the donating orbital leads to less stabilization when this orbital is mixed in with the virtuals of the substrate. The result is a diminished orbital interaction term, raising the energy profile. In more chemical terminology: stabilizing this occupied orbital leads to a smaller amount of charge donation into the antibonding $\sigma^*_{C—H}$ orbital, thereby hampering the bond-breaking process.

Without going into details here, we like to add for completeness that this effect of $\pi$-accepting ligands is only valid for catalysts that primarily interact with the substrate via donation from their d orbitals. This is true for most Pd-based catalysts, and we have designated this the d regime, as opposed to the s regime. In the latter, catalyst activity depends primarily on the s-accepting capability of the catalyst, and ligands can have completely opposite effects.[47]

In practice, the catalyst is often a dicoordinated species, and therefore the addition of the methane C—H bond to $Pd(PH_3)_2$ has also been subjected to activation strain analyses (red lines in Figure 4). Introduction of the second ligand leads to significant changes in the energy profile: immediately in the beginning it raises approximately 20 kcal $mol^{-1}$. After this initial increase, the profile is rather flat, but the reaction barrier is nevertheless much higher than for Pd and $PdPH_3$, and the overall reaction is more endothermic as well. Note also that it occurs more to the reactant side than the transition state for $PdPH_3$, that is, it shows anti-Hammond behavior. Again, we will discuss the strain and interaction energy components of the energy profile individually.

Starting with the strain energy, Figure 4 clearly shows that herein lies the origin of the sudden rise of the energy profile in the beginning of the reaction. Dissecting this term into individual contributions from the catalyst and the substrate reveals that the substrate deformation is rather similar for all reactions, as the character of its geometrical transformation is still very much unchanged. However, for the addition to $Pd(PH_3)_2$ a significantly larger catalyst contribution is found. Visual inspection of molecular geometries along the energy profile reveals that, in the beginning of the reaction, the phosphine ligands bend away to make room for the approaching substrate. This bending of the catalyst's bite angle is the origin of the increase in the strain term, and can be further rationalized using the Walsh diagram shown in Figure 5(a) for the general case of bisligated $d^{10}$-$ML_2$ transition metal complexes. Decreasing the L–M–L angle turns on the antibonding overlap of the ligand lone pairs with the $d_{xz}$ orbital, pushing it up in energy, while other orbitals are less strongly affected. The high-energy $b_1$ orbital also has a second, smaller effect on the energy profile, which shows up in the interaction energy term. This curve descends more steeply for $Pd(PH_3)_2$, because of the better electron-donating capabilities of this destabilized orbital. Combined, these two effects reveal the origin of the observed anti-Hammond behavior; compared with $PdPH_3$, the steeper descending interaction

  

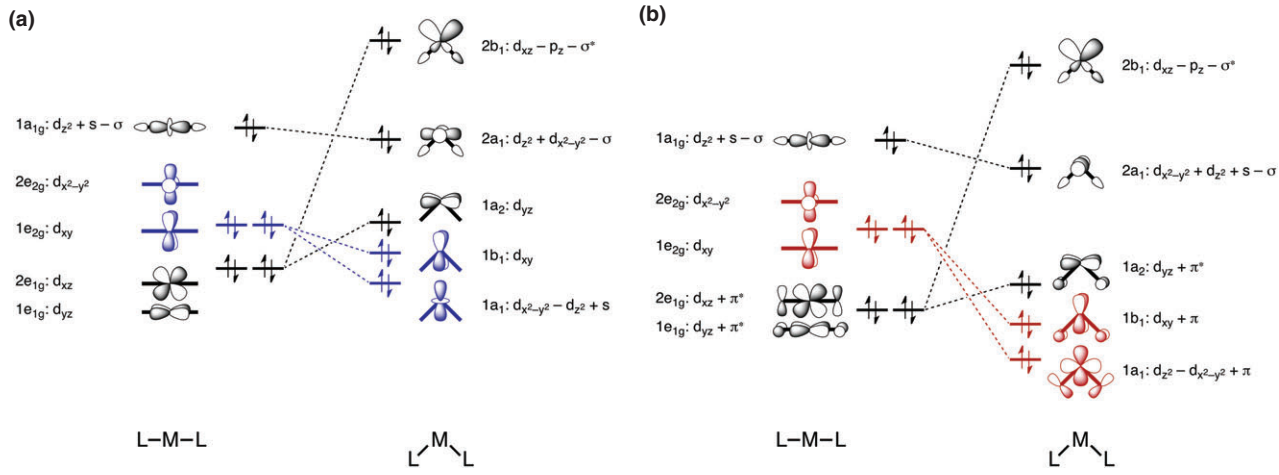


**FIGURE 5 |** Simplified Walsh diagrams for bending $ML_2$ complexes (a) without and (b) with $\pi$ backbonding, as they emerge from Kohn–Sham MO analyses (+/– indicate bonding/antibonding). A more detailed scheme of the intermixing occurring for the $a_1$ orbitals is available in the supporting information of Ref 87.

energy curve for $Pd(PH_3)_2$ shifts the transition state to the left, but it nevertheless occurs at a higher energy because the entire energy profile is, already from the beginning of the reaction, pushed up due to the additional strain energy that is required for bending away the ligands.

## Bite Angles and Their Flexibility in Transition Metal-Mediated Bond Activation

An important class of ligands used is that of chelating phosphine ligands, where the coordinating phosphine sites are connected by a polymethylene bridge. By varying the length of this bridge, one can obtain catalysts with different P–Pd–P bite angles. It is well-known that a smaller bite angle leads to an improved rate for the oxidative addition step.[127] Activation strain analyses on a series of chelating palladium-phosphine catalysts $Pd[PH_2(CH_2)_nPH_2]$ have revealed[43,44] the origin of this bite-angle effect. Selected results of these analyses are shown in Figure 6, where the results for Pd and $Pd(PH_3)_2$ are compared with the Pd complex with a chelating ligand, $Pd[PH_2(CH_2)_2PH_2]$, having a bite angle of only 98°. From these analyses it can be concluded that the lower reaction barriers for complexes with smaller bite angles originate from a softer strain term. This is closely related to the effect on this component described for the $Pd(PH_3)_2$ catalyst in the previous section: when a catalyst complex with a smaller bite angle is applied, there is less need to bend away the phosphine ligands. The reduced need for catalyst deformation prevents the strain energy term to rise in the beginning of the reaction, as found for $Pd(PH_3)_2$.

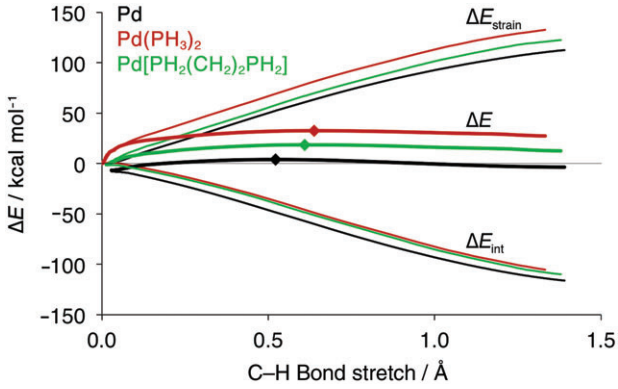


**FIGURE 6 |** Activation strain analyses for the oxidative addition of methane to Pd, $Pd(PH_3)_2$, and $Pd[PH_2(CH_2)_2PH_2]$. A dot designates a TS. Energies and bond stretch are relative to reactants.

Note that the analyses clearly reveal that this geometric effect is the reason for the lower barriers, that is, the bite-angle effect on reaction barriers results from steric reasons. The stronger donation from the destabilized $b_1$ orbital (see Figure 5) leads to a slightly improved catalyst–substrate interaction, but plays only a minor role.

Other studies have investigated the effect of using catalysts with metal centers other than Pd,[42,47] such as the $d^{10}$-$ML_2$ catalysts $Ni(PH_3)_2$ and $Pt(PH_3)_2$ (see Figure 7). Although all three catalyst complexes are rather similar, activation strain analyses revealed intriguing differences in both the strain and interaction terms. First, the weaker interaction for the Pd catalyst results mainly from the electron-donating capabilities: $Ni(PH_3)_2$ is a better electron donor than $Pd(PH_3)_2$ due to its higher-energy d-derived orbitals, whereas $Pt(PH_3)_2$ has larger d-derived orbitals that provide

  

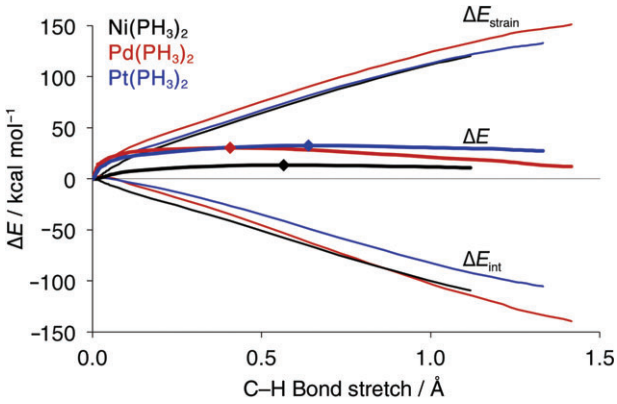


**FIGURE 7** | Activation strain analyses for the oxidative addition of methane to $Ni(PH_3)_2$, $Pd(PH_3)_2$, and $Pt(PH_3)_2$. A dot designates a TS. Energies and bond stretch are relative to reactants.

better overlap with the substrate $\sigma^*_{C—H}$ orbital. Second, the relatively low barrier for $Ni(PH_3)_2$ is also partly the result of a softer strain term, already in an early stage of the reaction, originating from the catalyst's contribution. Surprisingly, it appears that bending $Ni(PH_3)_2$ comes with a smaller energy penalty than bending the isoelectronic $Pd(PH_3)_2$ or $Pt(PH_3)_2$. Thus, there is a 'bite-angle effect', even though all three $M(PH_3)_2$ catalyst complexes have linear equilibrium geometries and their L–M–L angles are decreased to similar values in the course of the oxidative addition. This result indicates that the bite angle itself is not necessarily sufficient to predict the activity of the catalyst. Considering the bite-angle flexibility, that is the ease of decreasing the bite angle of a catalyst, gives better insights into catalyst activity.[47]

Yet, one may wonder why bending $Ni(PH_3)_2$ is more feasible than bending, for example, $Pd(PH_3)_2$. This issue has been addressed in a study on a large set of $d^{10}$-$ML_2$ catalyst complexes.[46,87] The systematic approach taken revealed a number of interesting trends, which we will address using two representative series, namely $Rh(PH_3)_2^-$, $Pd(PH_3)_2$, $Ag(PH_3)_2^+$ in which the metal center is varied, and $Pd(NH_3)_2$, $Pd(PH_3)_2$, $Pd(CO)_2$ in which the ligand is varied. It is found that the bite angle becomes less flexible when the metal center is varied from $Ag^+$ to $Rh^-$, and increasingly flexible from $Pd(NH_3)_2$ to $Pd(CO)_2$. In fact, the most flexible complexes from these series even have nonlinear equilibrium geometries. $Rh(PH_3)_2^-$ was found to have an intrinsically bent L–M–L angle of 141.2°, whereas $Pd(CO)_2$ has an L–M–L angle of 155.6°. Thus, as the metal center is varied from the poor electron-donating $Ag^+$ to Pd and the excellent electron-donating $Rh^-$, there is enhanced bite-angle flexibility. In addition, when the ligand is varied from the poor $\pi$-accepting $NH_3$ to the moderate $\pi$-accepting $PH_3$ to the excellent $\pi$-accepting CO, we find increased bite-angle flexibility. Detailed MO analyses revealed that $\pi$ backbonding is indeed of decisive importance for the observed bite-angle flexibility. This follows from a close inspection of the Walsh diagrams shown in Figure 5. Figure 5(a) shows the Walsh diagram for bending $ML_2$ complexes, as commonly found in textbooks.[97] In this diagram, the ligands are considered pure $\sigma$ donors. We have extended this with a second Walsh diagram (shown in Figure 5(b)), for the case of $\pi$-accepting ligands. In the latter, bending results in a significant $\pi$-backbonding stabilization of the lower $a_1$ and $b_1$ orbitals (indicated in red). If this effect is sufficiently strong, it compensates the destabilization of the $d_{xz}$-derived $b_1$ orbital, and results in nonlinear equilibrium geometries. This is the case for $Rh(PH_3)_2^-$ and $Pd(CO)_2$, and indeed even more so for $Rh(CO)_2^-$, which has a ligand–metal–ligand angle of only 130.8°. For $Ni(PH_3)_2$ and $Pd(PH_3)_2$, the effect is not strong enough to lead to a nonlinear equilibrium geometry, but the additional stabilization of the lower $a_1$ and $b_1$ orbitals at smaller bite angles nevertheless softens the resistance against bending. This effect is stronger for $Ni(PH_3)_2$, because the nickel metal center (which, in the complex, has a $d^{10}s^0$ valence configuration) has energetically higher d orbitals, and therefore stronger $\pi$ backbonding with the $PH_3$ ligands.

## Oxidative Addition of Different C—X Bonds to Palladium

So far, we have discussed examples in which the catalyst complex is modified, while keeping methane as the model substrate. Numerous studies have focused on variations in the substrate.[2,35–37,41,128] We will discuss the addition of different bonds to bare Pd, that is, besides the methane C—H bonds, also the C—X bonds from the series of halomethanes $CH_3F$, $CH_3Cl$, and $CH_3Br$.[41] Initially, one might expect that the barriers for Pd-mediated C—H and C—F activation are rather similar due to the similar bond dissociation energies of these bonds, and that the barriers for activating the weaker $CH_3$—Cl and $CH_3$—Br bonds are lower. Thus, in terms of the activation strain model, these expectations would show up in the strain energy term. Figure 8 confirms these expectations, although only partly.

Along the reaction coordinate, the strain energy curves are indeed lower for addition of the $CH_3$—Cl and $CH_3$—Br bonds, which is a direct consequence of these bonds being weaker than the $CH_3$—H and $CH_3$—F bonds, which have roughly similar homolytic bond dissociation energies. For all four reactions, the

  

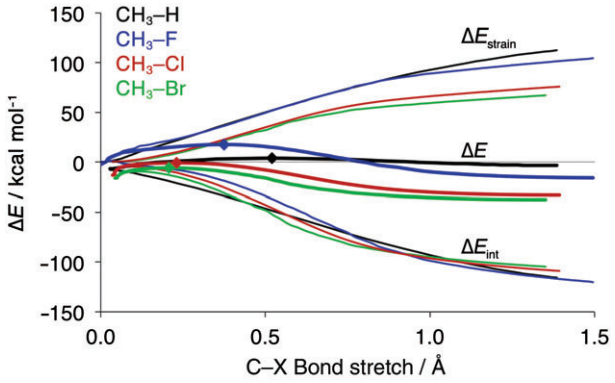


**FIGURE 8 |** Activation strain analyses for the oxidative addition of methane and halomethanes to Pd. A dot designates a TS. Energies and bond stretch are relative to reactants.

strain curve is reminiscent to the dissociation curve for the bond being activated. However, this does not directly translate into the C—H activation barrier being similar to that of C—F, and both being higher than the barriers for C—Cl and C—Br activation. In fact, the methane addition barrier is lower than that of fluoromethane and closer to those of chloromethane and bromomethane. As shown in Figure 8, this is because early during the reaction the interaction energy curve for C—H activation is more stabilizing than the interaction energies for carbon–halogen bond activation.

While the Pd—$CH_4$ interaction gains in strength immediately at the beginning of the addition process, the interaction curves for the halomethanes 'lag behind', that is, are initially weaker but later on descend more steeply and arrive at equal, and even lower values. This lag is caused by the different orbital-electronic structure of the halomethane substrates as compared with methane. For each reaction, a significant part of the interaction results from donation from the Pd d orbitals to the antibonding $\sigma^*$ orbital of the bond being broken. Shown below in Figure 9 are the different overlap situations for a Pd d orbital with (a) a C—H $\sigma^*$ orbital and (b) a $\sigma^*$ orbital of C—X and a stretched C—X bond. For methane, the $\sigma^*_{C—H}$ orbital consists of the out-of-phase combination of the $CH_3^\bullet$ $sp^3$ lobe (again, '$sp^3$' serves merely as a general description of this orbital's shape and is not used in its strictly formal sense) with the $H^\bullet$ 1s orbital, while for the halomethanes the $\sigma^*_{C—X}$ orbital is the out-of-phase combination of the $CH_3^\bullet$ $sp^3$ lobe with the halogen $X^\bullet$ *n*p orbital. The latter has an additional nodal plane centered at the halogen X, leading to partial cancelation of overlap with the Pd d orbitals in the beginning of the reaction, and a diminished (orbital) interaction energy. This delay in the build-up of stabilizing interactions causes the C—F activation barrier to be much higher than the C—H activation barrier, despite the similar bond strength. Later on, at larger C—X bond stretch (around 0.5 Å), the $\Delta E_{int}$ curve for C—X activation catches up, as the Pd d orbitals then also favorably overlap with the $\sigma^*_{C—X}$ orbital, leading to a strengthening of the interaction energy. This effect shows up not only when going from the C—H to the C—X bonds, but also along the C—X bonds from C—F to C—Cl to C—Br, which have increasingly stabilizing interaction energy curves. For the larger halogen atoms, less bond stretch is needed before good overlap with the Pd d orbital is achieved, and therefore the lag in the interaction energy term becomes less pronounced along this series. This is furthermore accompanied by the increased electron-accepting capability from the $\sigma^*_{C—F}$ to the $\sigma^*_{C—Br}$ orbitals, due to a lowering of the orbital energy along this series.

Thus, using activation strain analyses, the variations among the reaction barriers for C—H and C—X activation are readily explained using a combination of the bond dissociation energies of the targeted bonds, as well as the orbital-electronic structure of the substrate. From these results, it is readily concluded that (and understood why!) it is often insufficient to consider only the bond dissociation energies of the bonds. For the series discussed here, this would give qualitatively correct results, that is, the

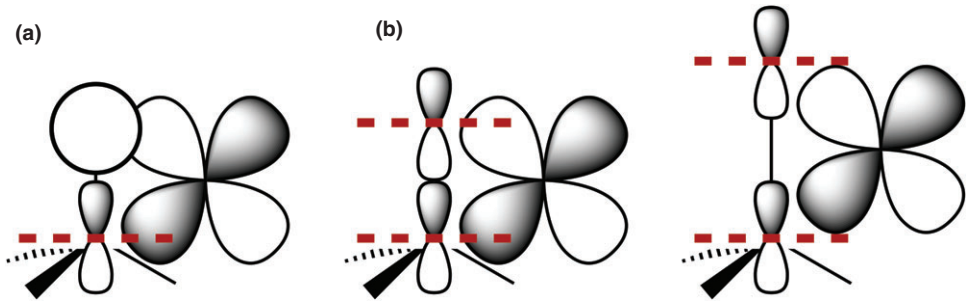


**FIGURE 9 |** Different overlap situations for the metal d orbital with (a) a carbon–hydrogen bond and (b) a carbon–halogen bond.

  

order of the reaction barriers would be predicted correctly. However, it is clear that a quantitative prediction of the reaction barriers, based solely on the BDE of the targeted bonds, would fail rather dramatically. When comparing the methane C—H bond and the ethane C—C bond, the situation would be even worse, as a prediction based on the bond dissociation energies would also fail qualitatively: although the C—C bond is weaker, cleaving it via oxidative addition to Pd goes with a higher barrier.[35] Also for this bond, with a $\sigma^*_{C-C}$ orbital that is the antibonding combination of two $CH_3^\bullet$ $sp^3$ lobes, this is due to the delayed build-up of stabilizing catalyst–substrate interactions. In a notable study on Pd-catalyzed cross coupling reactions involving a chloro aryl triflate as a coupling partner, Schoenebeck and Houk investigated the differences in electronic structure of C—Cl bond and C—OTf bonds and, combined with the ligand effects discussed above, were able to explain the regioselectivity observed.[129]

In the following, we will consider a different elementary chemical reaction in which halomethane C—X bonds are broken, namely, (backside) nucleophilic substitution, and draw a number of parallels derived from applying the activation strain model to both reactions and interpreting the results with MO theory. In principle, one could also describe the oxidative addition process as a frontside nucleophilic attack of the transition metal center at carbon, but for the sake of brevity we will not discuss this aspect here, and refer the reader to previous works dealing with this topic.[3,5,35,37,130]

## Leaving-Group Ability and Nucleophilicity in $S_N2$ Reactions

To arrive at a straightforward relationship between the electronic structure of the reactants and their $S_N2$ reactivity, a number of energy profiles have been investigated while systematically varying one of the reactants.[13] In Figure 10(a), we show the first of two representative series that we will discuss, namely the backside nucleophilic attack of $Cl^-$ on $CH_3X$ substrates, where the leaving group X in the substrate is varied along the halogens F to I. This gives the halomethanes $CH_3F$, $CH_3Cl$, $CH_3Br$, and $CH_3I$, thus resembling the series of C—X bonds in the last example of oxidative addition. Also in these $S_N2$ reactions, the C—X bond is broken by populating the $\sigma^*_{C-X}$ orbital, but now the electrons are being donated from the chloride nucleophile, which approaches the methyl moiety from the back, and not side-on like the Pd metal center in oxidative addition (the original study, Ref 13 also includes such frontside nucleophilic attacks).

It follows from these analyses that the leaving-group ability is directly determined by the C—X bond strength. Again, as from $CH_3F$ to $CH_3I$ the C—X bond strength decreases, the strain terms become less destabilizing, but now this directly translates into lower reaction barriers and more exothermic reactions. The differences between the interaction energy curves that were observed for the oxidative addition of these bonds (due to lagging, see Figure 8 in the previous section) are not observed here, because the nucleophile approaches from the back and has comparable overlap with the back-lobe of the $\sigma^*_{C-X}$ orbital for each substrate.

In Figure 10(b) the $S_N2$ energy profiles are compared for the reactions of different nucleophiles ($F^-$, $Cl^-$, $Br^-$, and $I^-$) with $CH_3Cl$. Along this series the leaving group is kept constant, which makes all strain curves essentially coincide. But, as the nucleophile is varied from $F^-$ to $I^-$ the interaction term becomes significantly less stabilizing, resulting in higher, more product-like reaction barriers, and less exothermic reaction energies. This is not only caused by the more diffuse charge distributions of the larger halogens,

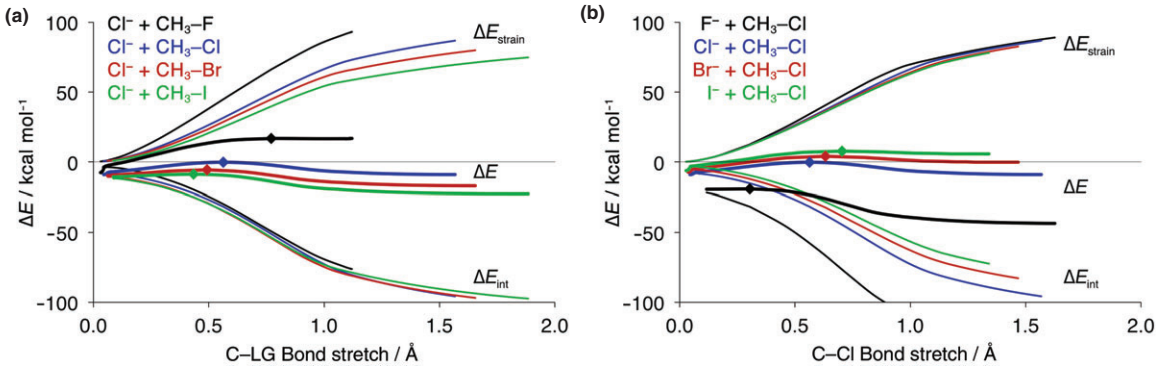


**FIGURE 10** | Activation strain analyses of the $S_N2$ reaction profiles for variation of (a) the leaving group and (b) the nucleophile. A dot designates a TS. Energies and bond stretch are relative to reactants.

  

but also a direct consequence of the electron-donating capability of the nucleophiles. This capability is reduced because of the decreasing *n*p orbital energies from $F^-$ to $I^-$, and therefore larger HOMO–LUMO energy gap with the substrate $\sigma^*_{C—Cl}$ orbital.

The analyses on the trends for leaving-group ability and nucleophilicity readily explain what makes for a good leaving group, or a good nucleophile, and how and why these properties translate into a lower $S_N2$ reaction barrier. Combined, by using for example a good nucleophile (such as $F^-$) and a substrate with a good leaving group (such as $CH_3I$), the barrier even vanishes entirely. However, for most $S_N2$ reactions $Nu^- + CH_3X$, a transition state occurs, due to the steric congestion that arises as five substituents try to bind to the central carbon atom.[10,104] This steric congestion can be lowered by going to a larger central atom, such as silicon, which forms stable five-coordinate compounds. Increasing the steric congestion by introducing bulky substituents R in $Cl^- + SiR_3Cl$ can cause $S_N2$ reaction barriers to reappear.[11,131] Similar results have been obtained for $S_N2$ at phosphorus centers.[10,132]

## From Nucleophilicity to Halophilicity and Protophilicity

Proceeding from the $Cl^- + CH_3Cl$ reactions, one can also replace the central $CH_3^\bullet$ moiety with an isolobal halogen atom. This reduces the steric interactions with the incoming base substantially, and results in a disappearance of the reaction barrier. Thus, we arrive at a set of halogen bond formation reactions between halides $X^-$ and dihalides YZ, which form stable halogen-bonded trihalides $[X–Y–Z]^-$. These halogen-bond formations have also been subject of detailed activation strain analyses and interpretation in terms of MO theory (X, Y, Z = F, Cl, Br, or I).[133] Like oxidative addition and nucleophilic substitution, also halogen-bond formation can be described as a donor–acceptor interaction, stemming to a large extent from charge being transferred from a Lewis base to the halogenated compound.[133–137] For the series studied, this stems from HOMO–LUMO interactions between the *n*p lone pair on $X^-$ and the $\sigma^*$ orbital on YZ. Not surprisingly, the results from this study therefore reveal many parallels to those discussed for $S_N2$ reactions between halides and halomethanes. Thus, stronger Lewis bases (i.e., better nucleophiles) form stronger halogen bonds due to stronger interactions, partly due to their better electron-donating capability. Also, halogen bonds $X^-\cdots YZ$ become stronger as the YZ dissociation curves become softer, as this induces less deformation (lower $\Delta E_{strain}$ curve), while at the same time a larger stretch of this bonds leads to a greater stabilization of the $\sigma^*_{Y—Z}$ orbital, and thereby enhances its electron-accepting capability.

One can go a step further and replace the central halogen atom with a hydrogen atom, to arrive at an analogous set of hydrogen-bond formations $X^- + HY \rightarrow [X–H–Y]^-$. Again, an important driving force behind these reactions is the HOMO–LUMO interaction between the *n*p lone pair on $X^-$ and the empty $\sigma^*$ orbital on HY, and the analyses revealed many parallels with $S_N2$ reactivity and halogen bonds.[133] The smaller hydrogen leads to even less steric repulsion than a larger central halogen. Interestingly, however, this does not necessarily mean that hydrogen bonds are stronger, because the $\sigma^*_{H—Y}$ orbitals on hydrogen halides are higher in energy and therefore less good acceptor orbitals than those on dihalides. This leads to less stabilizing (orbital) interactions in the case of hydrogen bonds. Furthermore, as hydrogen halide H—Y bonds are much stronger than dihalide Z—Y bonds, the H—Y bonds typically stretch less, hampering the build-up of stabilizing interactions. Essentially, this comes down to a decreased leaving-group ability of the halogen Y when it is connected to a hydrogen, compared with the same halogen Y connected to another halogen atom.

## Competition between $S_N2$ and E2 Reaction Mechanisms

In a recent study,[19] we compared the $S_N2$ energy profiles for $OH^- + CH_3CH_2OH$ and $H_2O + CH_3CH_2OH_2^+$ (see Figure 11, blue lines). This constitutes the effect of changing simultaneously from a model system with a good nucleophile and a poor leaving group ($OH^-$) to a model system with a poor nucleophile and an excellent leaving group ($H_2O$), by simply protonating both moieties. In agreement with the results discussed above, going from the $OH^-$ to the poorer $H_2O$ nucleophile weakens the interaction energy significantly, but this effect is almost entirely compensated for by the softer strain energy term, as simultaneously the leaving-group ability is enhanced from $CH_3CH_2OH$ to $CH_3CH_2OH_2^+$. The net result is only a small difference in reaction barrier, with the barrier for the protonated reaction being a few kcal $mol^{-1}$ lower.

The main reason to include this study here, however, is to provide an example on how the activation strain model is applied to compare two different reaction mechanisms that are in mutual competition. This study aimed specifically at revealing the origin of the often observed shift from elimination to substitution mechanism when the reaction conditions are changed from basic to acidic.

  

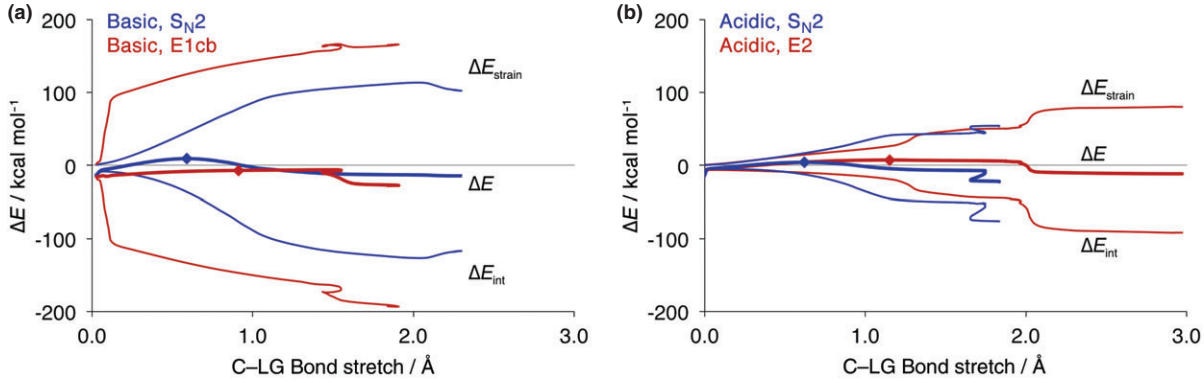


**FIGURE 11 |** Activation strain analyses of the model substitution and elimination reaction profiles under (a) basic ($OH^- + CH_3CH_2OH$) and (b) acidic ($H_2O + CH_3CH_2OH_2^+$) conditions. A dot designates a TS. Energies and bond stretch are relative to reactants.

We have compared the model $S_N2$ reactions between $OH^-$ and $CH_3CH_2OH$ and between $H_2O$ and $CH_3CH_2OH_2^+$ with the competitive base-induced 1,2-elimination reactions for the same pairs of reactants. The resulting four reactions resemble the substitution and elimination reactions under extremely basic ($OH^-$ as nucleophile or base) and acidic conditions ($H_2O$ as nucleophile or base). The results revealed indeed the experimentally observed shift from an elimination to a substitution pathway when changing from basic to acidic conditions. From an activation strain model perspective, the elimination pathway is generally expected to go with higher reaction barriers, due to the greater deformation of the reactants. In both $S_N2$ and E2 reactions, the C($\alpha$)—LG bond is broken, but E2 requires the additional rupture of a C($\beta$)—H bond, where $\alpha$ and $\beta$ refer to the positions of the carbon atoms relative to the leaving group LG. Only when the interaction energy is strong enough to overcome the extra strain energy, the elimination pathway (via an E1cb mechanism) becomes favored. For the strong base $OH^-$ this is the case, but not for the much weaker base $H_2O$, as shown in Figure 11. Owing to the significant loss of stabilizing interactions ($\Delta E_{int}$ curves) upon going from the elimination pathway under basic conditions to the acidic conditions, the preference shifts from protophilic attack for $OH^-$ to nucleophilic attack for $H_2O$.

There is, however, yet another reason behind this shift in preferred mechanism, caused by the different nature of the leaving groups present under both circumstances. This can be derived from a careful investigation of the electronic structure of the $CH_3CH_2OH$ and $CH_3CH_2OH_2^+$ substrates. In Figure 12, schematic MO diagrams are shown for these substrates, constructed from the fragments $CH_3^\bullet$ and $^\bullet CH_2OH$ or $^\bullet CH_2OH_2^+$.

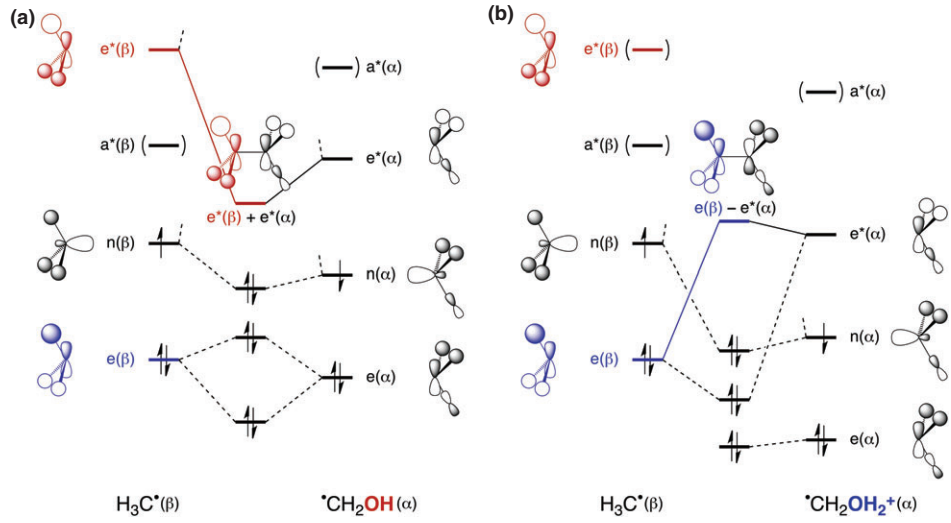


**FIGURE 12 |** Schematic substrate LUMO composition for (a) $CH_3CH_2OH$ and (b) $CH_3CH_2OH_2^+$.

  

In each reaction, the donor–acceptor interaction between an *n*p HOMO on the nucleophile/base and the substrate LUMO plays a key role. We will therefore focus exclusively on the LUMO for our discussion of the electronic structure of the substrates. First, note that for $CH_3CH_2OH$ the LUMO is, as commonly encountered, the $\pi$-bonding combination of the lowest unoccupied orbitals on both fragments, that is, the e*($\beta$) orbital on $CH_3^{\bullet}$, which has antibonding character along the C—H bond targeted by protophilic attack, and the e*($\alpha$) orbital on the $^{\bullet}CH_2OH$ fragment, which is antibonding along the carbon-leaving group bond. From here, it is easily seen that small variations in the leaving group will lead to small variations in the e*($\alpha$) orbital on the C($\alpha$) side of the substrate, and thereby change the relative amplitudes of the e* fragment orbitals in the overall LUMO. Thus, by stabilizing the e*($\alpha$) orbital, the LUMO gains amplitude on this side and reactivity is shifted toward $S_N2$.[1] However, this perturbative treatment breaks down when the e*($\alpha$) orbital is strongly stabilized due to the positive potential induced by the additional proton after protonation. As shown in Figure 12(b), the much lower e*($\alpha$) fragment orbital on $^{\bullet}CH_2OH_2^+$ interacts no longer with the $CH_3^{\bullet}$ e*($\beta$), but instead with the bonding e($\beta$) orbital. The resulting substrate LUMO is the $\pi$-antibonding combination, which has bonding character along the C—H bond targeted in the elimination pathway. Obviously, populating this bonding orbital does not contribute to $\beta$-proton transfer to the base, as required in the elimination pathway. The two extreme situations sketched above constitute an orbital electronic basis for an E2H–$S_N2$ mechanistic spectrum that may have E2C mechanisms somewhere in between.[1,138,139]

## CONCLUSION

When, after 7.5 million years of computing the supercomputer 'Deep Thought' finally gives Loonquawl and Phouchg the answer to 'The Great Question of Life, The Universe and Everything', the two men are perplexed as the computer simply says '42'. So goes the story of Douglas Adams' classic novel 'The Hitchhikers Guide to the Galaxy'.[140] Many computational chemists will, at least to a certain extent, be familiar with such situations. Nowadays it is relatively easy to run advanced computer simulations of chemical processes, and collect numerical data. The harder, but more interesting task of a computational chemist, is to give meaning to the numbers produced.

The activation strain model of chemical reactivity provides both qualitative and quantitative insight into energy profiles ($\Delta E$) of chemical processes by splitting the energy into a term stemming from geometrical deformation of the reactants ($\Delta E_{strain}$) and a term accounting for the mutual binding capabilities between the reactants ($\Delta E_{int}$). We have described, for example, how this approach has helped to separate the electronic effect from the steric effect of ligands in transition metal-catalyzed oxidative addition reactions, and understand both. This has lead to uncover that the bite-angle effect for these reactions is steric in nature. Furthermore, by comparing the activation of different bonds, it was shown that the barrier height for this process depends to a great extent on the catalyst's bonding capability, thereby explaining why the activity of a catalyst toward a certain bond is poorly predicted when only the strength of the targeted bond is considered. Interestingly, for bond rupture via an $S_N2$ mechanism, the bond strength can be used to predict reaction barrier heights, because these reactions are driven by a different orbital-electronic mechanism. Furthermore, applying the same methodology relates nucleophilicity of chemical species directly to basicity, and also to the stability of hydrogen- and halogen-bonded complexes in which these species participate.

Thus, these examples demonstrate how the activation strain model, combined with MO theory, provides insight into the essence of chemical reactivity and, importantly, how this yields powerful unifying concepts that enable rational tuning and design of molecular transformations across all branches of chemistry.

## REFERENCES


1. Bickelhaupt FM. Understanding reactivity with Kohn-Sham molecular orbital theory: E2-$S_N2$ mechanistic spectrum and other concepts. *J Comput Chem* 1999, 20:114–128.
2. de Jong GT, Bickelhaupt FM. Transition-state energy and position along the reaction coordinate in an extended activation strain model. *ChemPhysChem* 2007, 8:1170–1181.
3. van Zeist W-J, Bickelhaupt FM. The activation strain model of chemical reactivity. *Org Biomol Chem* 2010, 8:3118–3127.
4. Fernández I. Combined activation strain model and energy decomposition analysis methods: a new way


  

to understand pericyclic reactions. *Phys Chem Chem Phys* 2014, 16:7662–7671.

5. Fernández I, Bickelhaupt FM. The activation strain model and molecular orbital theory: understanding and designing chemical reactions. *Chem Soc Rev* 2014, 43:4953–4967.
6. Nagase S, Morokuma K. An ab initio molecular orbital study of organic reactions. The energy, charge, and spin decomposition analyses at the transition state and along the reaction pathway. *J Am Chem Soc* 1978, 100:1666–1672.
7. Strozier RW, Caramella P, Houk KN. Influence of molecular distortions upon reactivity and stereochemistry in nucleophilic additions to acetylenes. *J Am Chem Soc* 1979, 101:1340–1343.
8. Mitchell DJ, Schlegel HB, Shaik SS, Wolfe S. Relationships between geometries and energies of identity $S_N2$ transition states: the dominant role of the distortion energy and its origin. *Can J Chem* 1985, 63:1642–1648.
9. Ess DH, Houk KN. Distortion/interaction energy control of 1,3-dipolar cycloaddition reactivity. *J Am Chem Soc* 2007, 129:10646–10647.
10. van Bochove MA, Swart M, Bickelhaupt FM. Nucleophilic substitution at phosphorus ($S_N2$@P): disappearance and reappearance of reaction barriers. *J Am Chem Soc* 2006, 128:10738–10744.
11. Bento AP, Bickelhaupt FM. Nucleophilic substitution at silicon ($S_N2$@Si) via a central reaction barrier. *J Org Chem* 2007, 72:2201–2207.
12. Bento AP, Bickelhaupt FM. Frontside versus backside $S_N2$ substitution at group 14 atoms: origin of reaction barriers and reasons for their absence. *Chem Asian J* 2008, 3:1783–1792.
13. Bento AP, Bickelhaupt FM. Nucleophilicity and leaving-group ability in frontside and backside $S_N2$ reactions. *J Org Chem* 2008, 73:7290–7299.
14. Galabov B, Nikolova V, Wilke JJ, Schaefer HF III, Allen WD. Origin of the $S_N2$ benzylic effect. *J Am Chem Soc* 2008, 130:9887–9896.
15. Reyes L, Nicolás-Vázquez I, Mora-Diez N, Alvarez-Idaboy JR. Acid-catalyzed nucleophilic additions to carbonyl groups: is the accepted mechanism the rule or an exception? *J Org Chem* 2013, 78:2327–2335.
16. Pintér B, van Speybroeck V, Waroquier M, Geerlings P, de Proft F. Trans effect and trans influence: importance of metal mediated ligand–ligand repulsion. *Phys Chem Chem Phys* 2013, 15:17354–17365.
17. Mó O, Lamsabhi AM, Yáñez M, Heverly Coulson GS, Boyd RJ. Dramatic substituent effects on the mechanisms of nucleophilic attack on Se–S bridges. *J Comput Chem* 2013, 34:2537–2547.
18. Fernández I, Solà M, Bickelhaupt FM. Why do cycloaddition reactions involving $C_{60}$ prefer [6,6] over [5,6] bonds? *Chemistry* 2013, 19:7416–7422.
19. Wolters LP, Ren Y, Bickelhaupt FM. Understanding E2 versus $S_N2$ competition under acidic and basic conditions. *ChemistryOpen* 2014, 3:29–36.
20. Ess DH, Houk KN. Theory of 1,3-dipolar cycloadditions: distortion/interaction and frontier molecular orbital models. *J Am Chem Soc* 2008, 130:10187–10198.
21. Schoenebeck F, Ess DH, Jones GO, Houk KN. Reactivity and regioselectivity in 1,3-dipolar cycloadditions of azides to strained alkynes and alkenes: a computational study. *J Am Chem Soc* 2009, 131:8121–8133.
22. Agopcan S, Çelebi-Ölçüm N, Üçışık MN, Sanyal A, Aviyente V. Origins of the diastereoselectivity in hydrogen bonding directed Diels–Alder reactions of chiral dienes with achiral dienophiles: a computational study. *Org Biomol Chem* 2011, 9:8079–8088.
23. Paton RS, Kim S, Ross AG, Danishefsky SJ, Houk KN. Experimental Diels-Alder reactivities of cycloalkenones and cyclic dienes explained through transition-state distortion energies. *Angew Chem Int Ed* 2011, 50:10366–10368.
24. Garcia-Borràs M, Osuna S, Luis JM, Swart M, Solà M. The exohedral Diels–Alder reactivity of the titanium carbide endohedral metallofullerene $Ti_2C_2$@$D_{3h}$-$C_{78}$: comparison with $D_{3h}$-$C_{78}$ and $M_3N$@$D_{3h}$-$C_{78}$ (M = Sc and Y) reactivity. *Chemistry* 2012, 18:7141–7154.
25. Rajeev R, Sunoj RB. On the origin of regio- and stereoselectivity in singlet oxygen addition to enecarbamates. *J Org Chem* 2012, 77:2474–2485.
26. Hong X, Liang Y, Griffith AK, Lambert TH, Houk KN. Distortion-accelerated cycloadditions and strain-release-promoted cycloreversions in the organocatalytic carbonyl-olefin metathesis. *Chem Sci* 2013, 5:471–475.
27. Lu T, Wheeler SE. Origin of the superior performance of (thio)squaramides over (thio)ureas in organocatalysis. *Chemistry* 2013, 19:15141–15147.
28. Fernández I, Bickelhaupt FM. Origin of the "endo rule" in Diels–Alder reactions. *J Comput Chem* 2014, 35:371–376.
29. Fernández I, Solà M, Bickelhaupt FM. Origin of reactivity trends of noble gas endohedral fullerenes $Ng_2$@$C_{60}$ (Ng = He to Xe). *J Chem Theory Comput* 2014, 10:3863–3870.
30. Agopcan Cinar S, Ercan S, Erol Gunal S, Dogan I, Aviyente V. The origin of exo-stereoselectivity of norbornene in hetero Diels–Alder reactions. *Org Biomol Chem* 2014, 12:8079–8086.
31. Sarotti AM. Unraveling polar Diels–Alder reactions with conceptual DFT analysis and the distortion/interaction model. *Org Biomol Chem* 2014, 12:187–199.
32. Liu F, Liang Y, Houk KN. Theoretical elucidation of the origins of substituent and strain effects on the rates of Diels–Alder reactions of 1, 2, 4, 5-tetrazines. *J Am Chem Soc* 2014, 136:11483–11493.

  

33. Cao Y, Liang Y, Zhang L, Osuna S, Hoyt A-LM, Briseno AL, Houk KN. Why bistetracenes are much less reactive than pentacenes in Diels–Alder reactions with fullerenes. *J Am Chem Soc* 2014, 136:10743–10751.
34. Diefenbach A, Bickelhaupt FM. Oxidative addition of Pd to C-H, C-C and C-Cl bonds: importance of relativistic effects in DFT calculations. *J Chem Phys* 2001, 115:4030–4040.
35. Diefenbach A, Bickelhaupt FM. Activation of H-H, C-H, C-C, and C-Cl bonds by Pd(0). Insight from the activation strain model. *J Phys Chem A* 2004, 108:8460–8466.
36. Diefenbach A, Bickelhaupt FM. Activation of C-H, C-C and C-I bonds by Pd and cis-$Pd(CO)_2I_2$. Catalyst-substrate adaptation. *J Organomet Chem* 2005, 690:2191–2199.
37. Diefenbach A, de Jong GT, Bickelhaupt FM. Activation of H-H, C-H, C-C and C-Cl bonds by Pd and $PdCl^-$. Understanding anion assistance in C-X bond activation. *J Chem Theory Comput* 2005, 1:286–298.
38. Diefenbach A, de Jong GT, Bickelhaupt FM. Fragment-oriented design of catalysts based on the activation strain model. *Mol Phys* 2005, 103:995–998.
39. van Stralen JNP, Bickelhaupt FM. Oxidative addition versus dehydrogenation of methane, silane, and heavier $AH_4$ congeners reacting with palladium. *Organometallics* 2006, 25:4260–4268.
40. de Jong GT, Visser R, Bickelhaupt FM. Oxidative addition to main group versus transition metals: insights from the activation strain model. *J Organomet Chem* 2006, 691:4341–4349.
41. de Jong GT, Bickelhaupt FM. Catalytic carbon-halogen bond activation: trends in reactivity, selectivity, and solvation. *J Chem Theory Comput* 2007, 3:514–529.
42. de Jong GT, Bickelhaupt FM. Bond activation by group-11 transition-metal cations. *Can J Chem* 2009, 87:806–817.
43. van Zeist W-J, Visser R, Bickelhaupt FM. The steric nature of the bite angle. *Chemistry* 2009, 15:6112–6115.
44. van Zeist W-J, Bickelhaupt FM. Steric nature of the bite angle. A closer and a broader look. *Dalton Trans* 2011, 40:3028–3038.
45. Bäcktorp C, Norrby P-O. A DFT comparison of the neutral and cationic Heck pathways. *Dalton Trans* 2011, 40:11308–11314.
46. Wolters LP, Bickelhaupt FM. $d^{10}$-$ML_2$ complexes: structure, bonding, and catalytic activity. In: Eisenstein O, Macgregor S, eds. *Structure and Bonding*. Berlin, Heidelberg: Springer Berlin Heidelberg; 2014, DOI: 10.1007/430_2014_147.
47. Wolters LP, van Zeist W-J, Bickelhaupt FM. New concepts for designing $d^{10}$-$M(L)_n$ catalysts: d regime, s regime and intrinsic bite-angle flexibility. *Chemistry* 2014, 20:11370–11381.
48. Wang Y, Ahlquist MSG. Where does the water go? A computational study on the reactivity of a ruthenium(v) oxo complex (bpc)(bpy)$Ru^{V}O$. *Phys Chem Chem Phys* 2014, 16:11182–11185.
49. Joost M, Zeineddine A, Estevez L, Mallet-Ladeira S, Miqueu K, Amgoune A, Bourissou D. Facile oxidative addition of aryl iodides to gold(I) by ligand design: bending turns on reactivity. *J Am Chem Soc* 2014, 136:14654–14657.
50. El-Hamdi M, Tiznado W, Poater J, Solà M. An analysis of the isomerization energies of 1, 2-/1, 3-diazacyclobutadiene, pyrazole/imidazole, and pyridazine/pyrimidine with the turn-upside-down approach. *J Org Chem* 2011, 76:8913–8921.
51. Fernández I, Bickelhaupt FM, Cossío FP. Type-I dyotropic reactions: understanding trends in barriers. *Chemistry* 2012, 18:12395–12403.
52. El-Hamdi M, Solà M, Frenking G, Poater J. Comparison between alkalimetal and group 11 transition metal halide and hydride tetramers: molecular structure and bonding. *J Phys Chem A* 2013, 117:8026–8034.
53. El-Hamdi M, Farri El OEB, Salvador P, Abdelouahid BA, Begrani El MS, Poater J, Solà M. Analysis of the relative stabilities of ortho, meta, and para $MClY(XC_4H_4)(PH_3)_2$ heterometallabenzenes (M = Rh, Ir; X = N, P; Y = Cl and M = Ru, Os; X = N, P; Y = CO). *Organometallics* 2013, 32:4892–4903.
54. Contreras M, Osorio E, Ferraro F, Puga G, Donald KJ, Harrison JG, Merino G, Tiznado W. Isomerization energy decomposition analysis for highly ionic systems: case study of starlike $E_5Li_7^+$ clusters. *Chemistry* 2013, 19:2305–2310.
55. Castro AC, Osorio E, Cabellos JL, Cerpa E, Matito E, Solà M, Swart M, Merino G. Exploring the potential energy surface of $E_2P_4$ clusters (E = Group 13 element): the quest for inverse carbon-free sandwiches. *Chemistry* 2014, 20:4583–4590.
56. Fernández I, Bickelhaupt FM, Cossío FP. Double group transfer reactions: role of activation strain and aromaticity in reaction barriers. *Chemistry* 2009, 15:13022–13032.
57. Shinisha CB, Sunoj RB. Transition state models for probing stereoinduction in Evans chiral auxiliary-based asymmetric aldol reactions. *J Am Chem Soc* 2010, 132:12319–12330.
58. Lu T, Zhu R, An Y, Wheeler SE. Origin of enantioselectivity in the propargylation of aromatic aldehydes catalyzed by helical N-oxides. *J Am Chem Soc* 2012, 134:3095–3102.
59. Bronner SM, Mackey JL, Houk KN, Garg NK. Steric effects compete with aryne distortion to control regioselectivities of nucleophilic additions to 3-silylarynes. *J Am Chem Soc* 2012, 134:13966–13969.


  

60. Khan MAS, Zhang J, Sarma Das K, Ganguly B. Origins of reversing diastereoselectivity of α,β-dichloro-γ-butenolides and γ-butyrolactams in direct vinylogous aldol addition: a computational study. *RSC Adv* 2012, 2:8460–8466.
61. Kubas A, Bräse S, Fink K. Theoretical approach towards the understanding of asymmetric additions of dialkylzinc to enals and iminals catalysed by [2.2]paracyclophane-based N,O-ligands. *Chemistry* 2012, 18:8377–8385.
62. Li C-Q, Yang H-Q, Xu J, Hu C-W. Hydroxylation mechanism of methane and its derivatives over designed methane monooxygenase model with peroxo dizinc core. *Org Biomol Chem* 2012, 10:3924–3931.
63. Godin F, Prévost M, Gorelsky SI, Mochirian P, Nguyen M, Viens F, Guindon Y. Diastereoselective hydrogen-transfer reactions: an experimental and DFT study. *Chemistry* 2013, 19:9308–9318.
64. Kuribara T, Ishida S, Kudo T, Kyushin S. Microwave-assisted efficient one-pot synthesis of 9-phenyl-9,10-disilatriptycene and its bridgehead functionalization. *Organometallics* 2013, 32:2092–2098.
65. Pardue DB, Gustafson SJ, Periana RA, Ess DH, Cundari TR. Computational study of carbon–hydrogen bond deprotonation by alkali metal superbases. *Comp Theor Chem* 2013, 1019:85–93.
66. Medina JM, Mackey JL, Garg NK, Houk KN. The role of aryne distortions, steric effects, and charges in regioselectivities of aryne reactions. *J Am Chem Soc* 2014, 136:15798–15805.
67. Fernández I, Bickelhaupt FM, Cossío FP. Ene-ene-yne reactions: activation strain analysis and the role of aromaticity. *Chemistry* 2014.
68. Nava P, Carissan Y. On the ring-opening of substituted cyclobutene to benzocyclobutene: analysis of π delocalization, hyperconjugation, and ring strain. *Phys Chem Chem Phys* 2014, 16:16196–16203.
69. Jindal G, Sunoj RB. Axially chiral imidodiphosphoric acid catalyst for asymmetric sulfoxidation reaction: insights on asymmetric induction. *Angew Chem Int Ed* 2014, 53:4432–4436.
70. Orian L, van Stralen JNP, Bickelhaupt FM. Cyclotrimerization reactions catalyzed by Rhodium(I) half-sandwich complexes: a mechanistic density functional study. *Organometallics* 2007, 26:3816–3830.
71. Orian L, van Zeist W-J, Bickelhaupt FM. Linkage isomerism of nitriles in rhodium half-sandwich metallacycles. *Organometallics* 2008, 27:4028–4030.
72. Radius U, Bickelhaupt FM. Bonding of imidazol-2-ylidene ligands in nickel complexes. *Organometallics* 2008, 27:3410–3414.
73. Wassenaar J, Jansen E, van Zeist W-J, Bickelhaupt FM, Siegler MA, Spek AL, Reek JNH. Catalyst selection based on intermediate stability measured by mass spectrometry. *Nat Chem* 2010, 2:417–421.
74. Yang H-Q, Hu C-W, Gao C, Yang M-Y, Li F-M, Li C-Q, Li X-Y. Theoretical study on the gas-phase reaction mechanism between palladium monoxide and methane. *J Comput Chem* 2011, 32:3440–3455.
75. Lu G, Li H, Zhao L, Huang F, Schleyer PVR, Wang ZX. Designing metal-free catalysts by mimicking transition-metal pincer templates. *Chemistry* 2011, 17:2038–2043.
76. Weng C-M, Hong F-E. Density functional studies on diimine chelated palladium complex catalyzed Suzuki–Miyaura cross-coupling reaction: the impact of Lewis base employed in transmetallation process. *Dalton Trans* 2011, 40:6458–6468.
77. Qin S, Yang H-Q, Gao C, Xu J, Hu C-W. Methane dehydrogenation on monomeric Rh center located on (100) γ-alumina—a theoretical study. *Surf Sci* 2012, 606:1899–1905.
78. Li F-M, Yang H-Q, Ju T-Y, Li X-Y, Hu C-W. Activation of C–H and C–C bonds of ethane by gas-phase Pt atom: potential energy surface and reaction mechanism. *Comp Theor Chem* 2012, 994:112–120.
79. Gopakumar G, Belanzoni P, Baerends EJ. Hydroxylation catalysis by mononuclear and dinuclear iron oxo catalysts: a methane monooxygenase model system versus the Fenton reagent $Fe^{IV}O(H_2O)_5^{2}$. *Inorg Chem* 2012, 51:63–75.
80. Gorelsky SI, Lapointe D, Fagnou K. Analysis of the palladium-catalyzed (aromatic)C–H bond metalation–deprotonation mechanism spanning the entire spectrum of arenes. *J Org Chem* 2012, 77:658–668.
81. Gorelsky SI. Origins of regioselectivity of the palladium-catalyzed (aromatic) CH bond metalation–deprotonation. *Coordin Chem Rev* 2013, 257: 153–164.
82. Faza ON, Lopez CS, Fernández I. Noyori hydrogenation: aromaticity, synchronicity, and activation strain analysis. *J Org Chem* 2013, 78:5669–5676.
83. Liao W-H, Ho P-Y, Su M-D. Mechanisms for the reactions of group 10 transition metal complexes with metal-group 14 element bonds, $Bbt(Br)E=M(PCy_3)_2$ (E = C, Si, Ge, Sn, Pb; M = Pd and Pt). *Inorg Chem* 2013, 52:1338–1348.
84. Ju T-Y, Yang H-Q, Li F-M, Li X-Y, Hu C-W. Reaction mechanism on the activation of ethane C–H and C–C bonds by a diplatinum cluster. *Theor Chem Acc* 2013, 132:1387–1400.
85. Zhang C-G, Zhang L, Li H, Yu S-Y, Wang ZX. Differences between insertions of ethylene into metallocene and non-metallocene ethylene polymerization catalysts. *J Phys Org Chem* 2013, 26:70–76.
86. Orian L, Wolters LP, Bickelhaupt FM. In silico design of heteroaromatic half-sandwich $Rh^{I}$ catalysts for acetylene [2 + 2 + 2] cyclotrimerization: evidence of a reverse indenyl effect. *Chemistry* 2013, 19:13337–13347.


  

87. Wolters LP, Bickelhaupt FM. Nonlinear $d^{10}$-$ML_2$ transition-metal complexes. *ChemistryOpen* 2013, 2:106–114.
88. Joost M, Estevez L, Mallet-Ladeira S, Miqueu K, Amgoune A, Bourissou D. Mechanisms of syn-insertion of alkynes and allenes into gold–silicon bonds: a comprehensive experimental/theoretical study. *J Am Chem Soc* 2014, 136:10373–10382.
89. Fernández I, Wolters LP, Bickelhaupt FM. Controlling the oxidative addition of aryl halides to Au(I). *J Comput Chem* 2014, 35:2140–2145.
90. Xue L, Ahlquist MSG. A DFT study: why do $[Ni(P^R{}_2N^{R'}{}_2)_2]^{2+}$ complexes facilitate the electrocatalytic oxidation of formate? *Inorg Chem* 2014, 53:3281–3289.
91. Pintér B, Broeckaert L, Turek J, Růžička A, de Proft F. Dimers of N-heterocyclic carbene copper, silver, and gold halides: probing metallophilic interactions through electron density based concepts. *Chemistry* 2014, 20:734–744.
92. Woodward RB, Hoffmann R. The conservation of orbital symmetry. *Angew Chem Int Ed* 1969, 8:781–853.
93. Fukui K. Recognition of stereochemical paths by orbital interaction. *Acc Chem Res* 1971, 4:57–64.
94. Hoffmann R. Building bridges between inorganic and organic chemistry (Nobel Lecture). *Angew Chem Int Ed* 1982, 21:711–724.
95. Rauk A. *Orbital Interaction Theory of Organic Chemistry*. 2nd ed. New York: John Wiley & Sons; 2001.
96. Fleming I. *Molecular Orbitals and Organic Chemical Reactions, Reference Edition*. Chichester: John Wiley & Sons; 2010.
97. Albright TA, Burdett JK, Whangbo MH. *Orbital Interactions in Chemistry*. 2nd ed. Hoboken, NJ: John Wiley & Sons; 2013.
98. Bickelhaupt FM, Baerends EJ, Nibbering NMM. The effect of microsolvation on E2 and $S_N2$ reactions: theoretical study of the model system $F^- + C_2H_5F + n$ HF. *Chemistry* 1996, 2:196–207.
99. Hammond GS. A correlation of reaction rates. *J Am Chem Soc* 1955, 77:334–338.
100. van Zeist W-J, Koers AH, Wolters LP, Bickelhaupt FM. Reaction coordinates and the transition-vector approximation to the IRC. *J Chem Theory Comput* 2008, 4:920–928.
101. Bickelhaupt FM, Baerends EJ. The case for steric repulsion causing the staggered conformation of ethane. *Angew Chem Int Ed* 2003, 42:4183–4188.
102. Poater J, Solà M, Bickelhaupt FM. Hydrogen-hydrogen bonding in planar biphenyl, predicted by atoms-in-molecules theory, does not exist. *Chemistry* 2006, 12:2889–2895.
103. van Zeist W-J, Bickelhaupt FM. Trends and anomalies in H-$AH_n$ and $CH_3$-$AH_n$ bond strengths ($AH_n = CH_3$, $NH_2$, OH, F). *Phys Chem Chem Phys* 2009, 11:10317–10322.
104. van Zeist W-J, Bickelhaupt FM. Comment on "The interplay between steric and electronic effects in $S_N2$ reactions". *Chemistry* 2010, 16:5538–5541.
105. OED Online. Oxford University Press. Available at: http://www.oed.com/. (Accessed September 18, 2014).
106. Ayala FJ. *Science, Evolution, and Creationism*. Washington DC: The National Academies Press; 2008.
107. Bickelhaupt FM, Baerends EJ. Kohn-Sham density functional theory: predicting and understanding chemistry. In: Lipkowitz KB, Boyd DB, eds. *Reviews in Computational Chemistry*, vol. 15. New York: VCH Publishers Inc; 2000, 1–86.
108. Baerends EJ, Gritsenko OV, van Meer R. The Kohn–Sham gap, the fundamental gap and the optical gap: the physical meaning of occupied and virtual Kohn–Sham orbital energies. *Phys Chem Chem Phys* 2013, 15:16408–16425.
109. Reed AE, Curtiss LA, Weinhold F. Intermolecular interactions from a natural bond orbital, donor-acceptor viewpoint. *Chem Rev* 1988, 88:899–926.
110. Glendening ED, Streitwieser A. Natural energy decomposition analysis: an energy partitioning procedure for molecular interactions with application to weak hydrogen bonding, strong ionic, and moderate donor-acceptor interactions. *J Chem Phys* 1994, 100:2900–2909.
111. Jeziorski B, Moszynski R, Szalewicz K. Perturbation-theory approach to intermolecular potential-energy surfaces of van-der-Waals complexes. *Chem Rev* 1994, 94:1887–1930.
112. Blanco MA, Pendás AM, Francisco E. Interacting quantum atoms: a correlated energy decomposition scheme based on the quantum theory of atoms in molecules. *J Chem Theory Comput* 2005, 1:1096–1109.
113. Mitoraj MP, Michalak A, Ziegler T. A combined charge and energy decomposition scheme for bond analysis. *J Chem Theory Comput* 2009, 5:962–975.
114. Szalewicz K. Symmetry-adapted perturbation theory of intermolecular forces. *WIREs Comput Mol Sci* 2011, 2:254–272.
115. te Velde G, Bickelhaupt FM, Baerends EJ, Fonseca Guerra C, van Gisbergen SJA, Snijders JG, Ziegler T. Chemistry with ADF. *J Comput Chem* 2001, 22:931–967.
116. Hopffgarten MV, Frenking G. Energy decomposition analysis. *WIREs Comput Mol Sci* 2012, 2:43–62.
117. Morokuma K. Molecular orbital studies of hydrogen bonds. III. $C=O\cdots H$-O hydrogen bond in $H_2CO\cdots H_2O$ and $H_2CO\cdots 2H_2O$. *J Chem Phys* 1971, 55:1236–1244.
118. Kitaura K, Morokuma K. A new energy decomposition scheme for molecular interactions within the


  

Hartree-Fock approximation. *Int J Quantum Chem* 1976, 10:325–340.

119. Ziegler T, Rauk A. On the calculation of bonding energies by the Hartree Fock Slater method. 1. The transition state method. *Theor Chim Acta* 1977, 46:1–10.
120. Ziegler T, Rauk A. A theoretical study of the ethylene-metal bond in complexes between $Cu^+$, $Ag^+$, $Au^+$, $Pt^0$, or $Pt^{2+}$ and ethylene, based on the Hartree-Fock-Slater transition-state method. *Inorg Chem* 1979, 18:1558–1565.
121. Ziegler T, Rauk A. CO, CS, $N_2$, $PF_3$, and $CNCH_3$ as $\sigma$ donors and $\pi$ acceptors. A theoretical study by the Hartree-Fock-Slater transition-state method. *Inorg Chem* 1979, 18:1755–1759.
122. Bader RFW. Pauli repulsions exist only in the eye of the beholder. *Chemistry* 2006, 12:2896–2901.
123. Poater J, Solà M, Bickelhaupt FM. A model of the chemical bond must be rooted in quantum mechanics, provide insight, and possess predictive power. *Chemistry* 2006, 12:2902–2905.
124. Hoffmann R. *Solids and Surfaces*. New York: John Wiley & Sons; 1988.
125. Hartwig JF. *Organotransition Metal Chemistry: From Bonding to Catalysis*. Sausalito, CA: University Science Books; 2010.
126. de Jong GT, Geerke DP, Diefenbach A, Bickelhaupt FM. DFT benchmark study for the oxidative addition of $CH_4$ to Pd. Performance of various density functionals. *Chem Phys* 2005, 313:261–270.
127. van Leeuwen PWNM, Kamer PCJ, Reek JNH, Dierkes P. Ligand bite angle effects in metal-catalyzed C-C bond formation. *Chem Rev* 2000, 100:2741–2769.
128. de Jong GT, Kovacs A, Bickelhaupt FM. Oxidative addition of hydrogen halides and dihalogens to Pd. Trends in reactivity and relativistic effects. *J Phys Chem A* 2006, 110:7943–7951.
129. Schoenebeck F, Houk KN. Ligand-controlled regioselectivity in palladium-catalyzed cross coupling reactions. *J Am Chem Soc* 2010, 132:2496–2497.
130. Bickelhaupt FM, Ziegler T, Schleyer PVR. Oxidative insertion as frontside $S_N2$ substitution: a theoretical study of the model reaction system $Pd + CH_3Cl$. *Organometallics* 1995, 14:2288–2296.
131. Pierrefixe SCAH, Fonseca Guerra C, Bickelhaupt FM. Hypervalent silicon versus carbon: ball-in-a-box model. *Chemistry* 2008, 14:819–828.
132. van Bochove MA, Swart M, Bickelhaupt FM. Nucleophilic substitution at phosphorus centers (S(N)2@P). *ChemPhysChem* 2007, 8:2452–2463.
133. Wolters LP, Bickelhaupt FM. Halogen bonding versus hydrogen bonding: a molecular orbital perspective. *ChemistryOpen* 2012, 1:96–105.
134. Palusiak M. On the nature of halogen bond – the Kohn–Sham molecular orbital approach. *J Mol Struct* 2010, 945:89–92.
135. Stone AJ. Are halogen bonded structures electrostatically driven? *J Am Chem Soc* 2013, 135:7005–7009.
136. Pintér B, Nagels N, Herrebout WA, de Proft F. Halogen bonding from a hard and soft acids and bases perspective: investigation by using density functional theory reactivity indices. *Chemistry* 2013, 19:519–530.
137. Wolters LP, Smits NWG, Fonseca Guerra C. Covalency in resonance-assisted halogen bonds demonstrated with cooperativity in N-halo-guanine quartets. *Phys Chem Chem Phys* 2015, 17:1585–1592.
138. Parker AJ, Ruane M, Biale G, Winstein S. Elimination reactions. The E2C mechanism. *Tetrahedron Lett* 1968, 9:2113–2118.
139. Smith M. *March's Advanced Organic Chemistry*. 7th ed. Hoboken, NJ: John Wiley & Sons; 2013.
140. Adams D. *The Hitchhicker's Guide to the Galaxy*. London: Pan Books; 1979.

## FURTHER READING

Bickelhaupt FM. Understanding reactivity with Kohn-Sham molecular orbital theory: E2-$S_N2$ mechanistic spectrum and other concepts. *J Comput Chem* 1999, 20:114–128. [1]

Albright TA, Burdett JK, Whangbo MH. *Orbital Interactions in Chemistry*. 2nd ed. Hoboken, NJ: John Wiley & Sons; 2013. [97]

Hoffmann R. Building bridges between inorganic and organic chemistry (Nobel Lecture). *Angew Chem Int Ed* 1982, 21:711–724. [94]

Shaik SS, Hiberty PC. *A Chemist's Guide to Valence Bond Theory*. Hoboken, NJ: John Wiley & Sons; 2007.

  